

Bioinspired Molecular Bridging in a Hybrid Perovskite Leads to Enhanced Stability and Tunable Properties

Arad Lang, Iryna Polishchuk, Eva Seknazi, Jochen Feldmann, Alexander Katsman, and Boaz Pokroy*

Hybrid perovskites demonstrate high potential in optoelectronic applications. Their main drawback is their low stability under humid conditions. In this paper, one of nature's strategies is implemented—the incorporation of amino acids into the crystal lattice—in order to improve the stability of methylammonium lead bromide (MAPbBr₃) in water, and to tune its structure, as well as its optical and thermal properties. The amino acid lysine, which possesses two NH₃⁺ groups, is incorporated into the hybrid unit cell, by substituting two methylammonium ions and serves as a “molecular bridge”. This incorporation induces a decrease in the lattice parameter of the host, accompanied with an increase in its bandgap and noticeable changes in its morphology. Furthermore, a substantial decrease in the thermal expansion coefficient of MAPbBr₃ and a shift of its cubic-to-tetragonal phase transformation temperature are observed. Two different modes of incorporation are identified, which depend on the conditions of crystallization. These modes dictate the level of lysine incorporation and the magnitude of MAPbBr₃ bandgap changes. Notably, lysine incorporation strongly increases the perovskite stability in water. This study demonstrates a unique and promising approach to tune the properties and improve the stability of hybrid perovskites via this novel bioinspired route.

1. Introduction

In recent years, hybrid organic–inorganic perovskites (HOIPs)^[1–3] have attracted widespread attention due to their utility in various applications, such as photovoltaics,^[4–8] light emitting diodes (LEDs),^[9–11] and photodetectors.^[12–14] These HOIPs have been widely studied considering their exceptional conversion efficiency,^[8,15,16] together with easy bulk

synthesis,^[17–19] device fabrication,^[4,20] and bandgap engineering techniques.^[21]

One major setback which hinders HOIPs from being commercially used is their low stability.^[22,23] This family of materials is chemically active and thermally unstable.^[24,25] They tend to degrade and decompose while reacting with water (humidity),^[26,27] oxygen,^[28] and even light itself.^[29] In order to overcome this difficulty, many attempts have been done, among them adding organic^[30–32] or oxide^[33] protective layers, ion substitutions^[34,35] and morphology control.^[36–39] Given the remarkable potential of these systems and the importance of novel pathways to tune the physical properties of HOIPs, as well as to improve their stability, we were interested in the possibility of a Nature-inspired tuning strategy: via the incorporation of amino acids into HOIPs' crystal lattice and its effects on the crystal structure and properties.


Biomaterials, owing to their superior mechanical properties, have been a source of inspiration to scientists for many years.^[40–48] Common examples are mollusk shells, which are remarkably hard and tough,^[49–51] although they are composed of calcium carbonate (CaCO₃), a brittle ceramic. Such enhancement of mechanical properties originates from several factors, which include both intra- and intercrystalline organics along with unique hierarchical structures.^[49,52–54]

Interaction between the inorganic matrix and the organic inclusions (usually peptides or polysaccharides) in biomaterials is complex and is not yet fully understood.^[55,56] Calcite, the most thermodynamically stable polymorph of CaCO₃,^[57] was nevertheless shown to be capable of incorporating proteins,^[56,58] polymer nanoparticles,^[59,60] dyes,^[61] inorganic nanoparticles,^[62–64] graphene oxide,^[65] anticancer drugs,^[66] gels,^[67,68] and individual amino acids.^[69–71] Incorporation of amino acids induces expansion of the unit cell (i.e., an increase of the lattice parameters, both *a* and *c*), and is accompanied by significant changes in the crystal morphology.^[69,71–73] Furthermore, the incorporated amino acids enhance the hardness of the synthetic calcite single crystals, as they create internal stresses and act as precipitates in a second phase-hardening mechanism.^[70]

The ability to incorporate amino acids does not belong exclusively to calcite. Zinc oxide (ZnO, wurtzite) and copper oxide (Cu₂O, cuprite) were also shown to be capable of hosting

A. Lang, I. Polishchuk, E. Seknazi, A. Katsman, B. Pokroy
Department of Materials Science & Engineering and
the Russell Berrie Nanotechnology Institute
Technion–Israel Institute of Technology
Haifa 3200003, Israel
E-mail: bpokroy@technion.ac.il

J. Feldmann
Chair for Photonics and Optoelectronics
Nano-Institute Munich
Department of Physics
Ludwig-Maximilians-Universität (LMU)
Königinstr. 10, Munich 80539, Germany

 The ORCID identification number(s) for the author(s) of this article can be found under <https://doi.org/10.1002/adfm.202005136>.

DOI: 10.1002/adfm.202005136

individual amino acids.^[74,75] For ZnO the effect of the incorporation is similar to that of calcite; in both cases the unit cell expands, and there are changes in crystal morphology.^[74] In contrast, incorporation of amino acids into Cu₂O causes shrinkage of its unit cell, owing to substitution of the Cu²⁺ by the amine moiety of the amino acid.^[75] Interestingly, this incorporation induces an increase in the optical bandgaps of both of the inorganic semiconductors.^[74–76] This increase results from a quantum-size-like effect, in which localization of charge carriers is induced by dispersion of the insulating amino acids within the semiconducting matrix.^[76]

In this study, our material of choice from the HOIP family is methylammonium lead bromide (MAPbBr₃).^[10,11,77–80] It possesses the classic cubic perovskite ABX₃ structure, with CH₃NH₃⁺ (MA⁺) cations in its A-sites, which are asymmetric and randomly aligned.^[81,82] Incorporation of amino acids into the lattice structure of HOIPs has never been performed before. We therefore aimed to investigate whether such incorporation is feasible in this system, and if so, to determine its effects on the crystal structure and properties.

2. Results and Discussion

We synthesized MAPbBr₃ crystals from solution by utilizing the method described by Poglitsch and Weber.^[17] In a typical synthesis, a Pb²⁺ solution was prepared by dissolving lead acetate (Pb(OAc)₂) in concentrated hydrobromic acid (HBr). The same amount of all the 20 common L-amino acids were added to the Pb²⁺ solution. Precipitation of MAPbBr₃ was activated by the addition of an equimolar volume of MA⁺ solution to the Pb²⁺ solution (for more details see Experimental Section). Crystallization was achieved via two different routes: fast synthesis, in which the MA⁺ solution was added to the Pb²⁺ solution at room temperature while stirring, and slow synthesis, in which the MA⁺ solution was added to a hot Pb²⁺ solution (in an oil bath at 95 °C) and the mixture was cooled down in air. In both cases, the resulting orange-hued precipitates were filtered, washed with acetone, and dried in air.

As a first analysis of the precipitated crystals, we characterized their structure utilizing high-resolution powder X-ray diffraction (HR-PXRD). By applying Rietveld refinement^[83] on the full diffraction patterns we were able to deduce the lattice parameters of the crystals with high precision. When we compared the crystal structure of crystals formed with and without amino acids in the crystallization solution, lattice contraction

could be seen in the former case (Figure 1). Exceptions in this regard were Asn, Gln, and Trp. Asn and Gln were excluded because of spontaneous decomposition of the amide group in the acidic solution, and Trp was not soluble.

From Figure 1 (see also Table S1, Supporting Information), it is evident that by far the highest distortions are induced by lysine (Lys), indicating that this amino acid induces the most pronounced effect.^[69,74,75] Moreover, it is clear that the incorporation of other amino acids was lower, and was at approximately the same level in both growing routes. Since the effect of Lys on the MAPbBr₃ lattice was significantly higher, especially via the slow growth procedure, we focused in this work on the study of Lys incorporation. MAPbBr₃ samples were grown from solutions containing different Lys concentrations: 0.00, 0.02, 0.04, 0.06, and 0.08 g mL⁻¹.

After dissolving the crystals, we used amino acid analysis (AAA) to estimate the correlation between the concentration of incorporated Lys ([Lys]_{inc}) and its initial concentration in solution ([Lys]_{sol}) (Figure 1c). As expected, increasing the concentration of Lys in the Pb²⁺ solution (prior to addition of MA⁺ to the solution) resulted in a larger amount of incorporated Lys. It is also apparent from Figure 1c that the fast crystallization led to higher incorporation levels than those of the slow process, reaching a maximum of almost 1 mol%. In fact, the level of Lys incorporation into the lattice of MAPbBr₃ was of the same order of magnitude as that of Asp incorporated into calcite^[70] and of Asn incorporated into Cu₂O.^[75] More interestingly, HR-PXRD analysis revealed that the incorporation of Lys into MAPbBr₃ crystals induces a shift of the diffraction peaks to higher 2θ values (Figure 2a), which—according to Bragg's law^[84]—corresponds to smaller interplanar spacings. Similar lattice shrinkage rather than expansion was observed upon incorporation of amino acids into Cu₂O semiconductor.^[75] Plotting the lattice contraction as a function of incorporation levels (Figure 2b, Table S2, Supporting Information) clearly demonstrates that for both growth regimes, fast and slow, the higher the level of Lys incorporation, the higher the induced lattice shrinkage.

We also fitted a pseudo-Voigt function to the {100} diffraction peak of each sample and calculated the average grain size and microstrain fluctuations based on the full width at half maximum (FWHM, see Table S3, Supporting Information).^[85] As shown in Figure 2c, the microstrain fluctuations decreased with increasing amounts of Lys in the crystals. This trend differs from the widespread phenomenon in which the incorporation of organics is known to cause an increase in FWHM^[69,74] in biogenic crystals as well as in amino acid incorporated synthetic calcite.

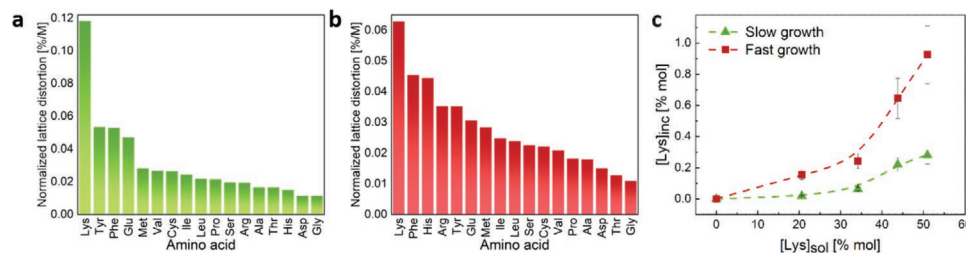


Figure 1. Normalized lattice distortions (absolute values) in MAPbBr₃ crystals induced during their growth in the presence of different amino acids: a) slow growth; b) fast growth. The normalized distortions are the measured distortions (using HR-PXRD) divided by the molarity of amino acid molecules in solution. c) Concentration of incorporated Lys (measured by AAA) versus its concentration in solution under conditions of slow and fast growth.

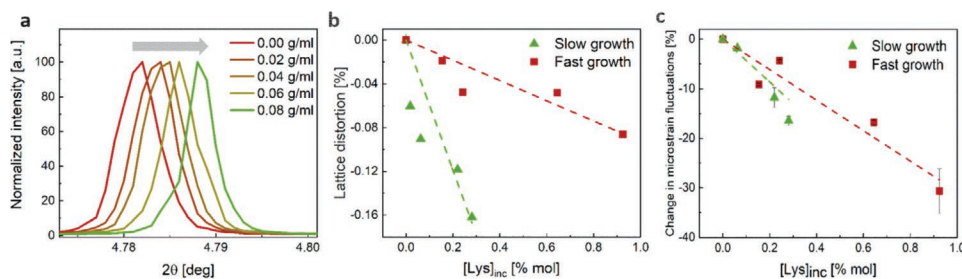


Figure 2. a) The {100} diffraction peak of MAPbBr₃ grown in the presence of different amounts of Lys ($\lambda = 0.49599 \text{ \AA}$). b) Lattice distortions and c) relative changes in microstrain fluctuations of MAPbBr₃ versus concentration of the incorporated Lys.

The incorporation of about 1 mol% of an amino acid into MAPbBr₃ has the potential to alter the thermal properties of the host crystal. To verify this assumption, the lattice parameter of each sample was measured via HR-PXRD coupled with in situ cooling at different temperatures (290, 275, 250, and 230 K—see Figure S4, Supporting Information). Cooling was achieved using a cold nitrogen gas blower. The thermal expansion coefficient was calculated according to Equation (1)

$$\alpha_L \equiv \frac{1}{a} \frac{\partial a}{\partial T} = \frac{\partial \ln a}{\partial T} \quad (1)$$

where a is the measured lattice parameter. By plotting the slope of $\ln(a)$ versus the absolute temperature, the thermal expansion coefficient can be extracted.

In the case of Lys incorporation, a noticeable effect on the thermal properties of MAPbBr₃ was observed, namely a decrease in the thermal expansion coefficient (Figure 3a) with increasing Lys concentration. For changes in lattice parameter, the relation between the change in thermal expansion coefficient and the lattice contraction can be estimated as

$$\frac{\alpha_L - \alpha_L^0}{\alpha_L^0} = -\frac{\frac{3Qa_0}{K} \left(\frac{\Delta a}{a_0}\right)}{1 + \frac{3Qa_0}{K} \left(\frac{\Delta a}{a_0}\right)} \approx -\frac{3Qa_0}{K} \left(\frac{\Delta a}{a_0}\right) \quad (2)$$

where Q and K are coefficients of the power series expansion of the interatomic potential, and $\Delta a/a_0$ is the (negative) lattice

distortion (for more details, see Supporting Information). According to Equation (2), the change in thermal expansion coefficient is proportional to the lattice distortion. This result can explain both the trend and the difference between slow- and fast-grown MAPbBr₃, as presented in Figure 3.

MAPbBr₃ is known to undergo a cubic-to-tetragonal (C-T) phase transformation (from $Pm\bar{3}m$ to $I4/mcm$ space group) during cooling, at a temperature of about $-36 \text{ }^\circ\text{C}$.^[17] In light of this, and since Lys incorporation was found here to affect the thermal expansion properties of MAPbBr₃, we also studied the effect of incorporated Lys on the C-T phase transformation. To this end, using differential scanning calorimetry (DSC), we evaluated the phase transformation temperature of a control sample as well as of Lys-incorporated samples. Each sample was scanned from room temperature to $-80 \text{ }^\circ\text{C}$ and back, at a rate of $5 \text{ }^\circ\text{C min}^{-1}$. The transformation temperature was taken as the temperature at the onset of the phase transformation peak (see Figure S5a in the Supporting Information).

Interestingly, we found that the temperature of the C-T phase transformation was indeed altered upon the incorporation of Lys (Figure 4a). Relatively to the control sample, the transformation temperature of the Lys-incorporated samples decreased during heating and increased during the cooling cycle. The temperature of transformation of pure MAPbBr₃ is in good agreement with a previous report.^[17] It is clear, moreover, that this trend intensifies as the Lys incorporation level increases. Given that the incorporation occurs while MAPbBr₃ is crystallizing in its cubic form (above the transformation temperature), this finding was the opposite of what we would expect from

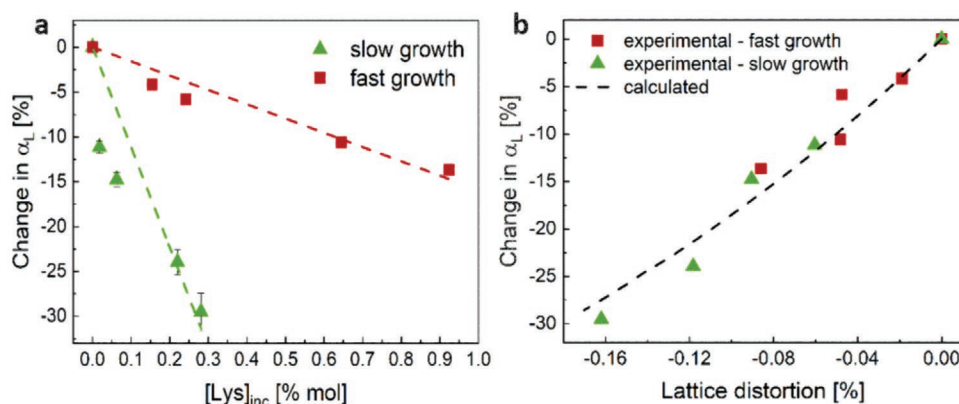


Figure 3. Change in MAPbBr₃ thermal expansion coefficient α_L versus a) concentration of incorporated Lys, and b) lattice distortion. The dashed line in (b) corresponds to Equation (2).

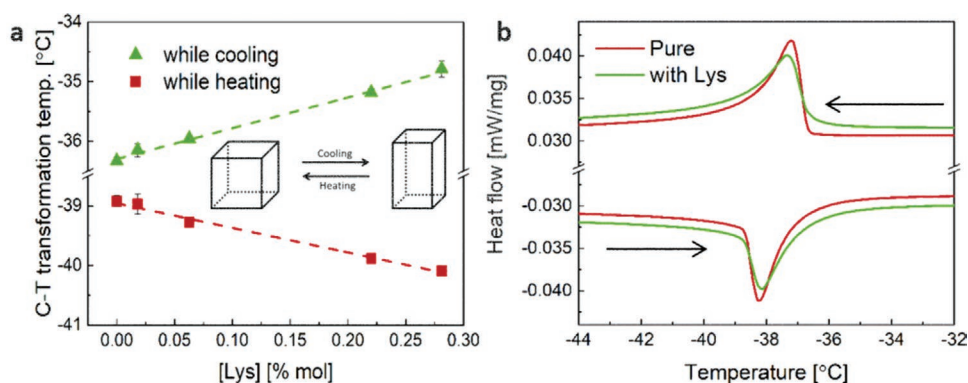


Figure 4. a) Phase transformation temperature of slow-grown MAPbBr₃ versus concentration of incorporated Lys, measured while cooling and heating using DSC. b) DSC curves of MAPbBr₃ around the phase transformation temperature, with and without incorporated Lys. The arrows indicate the direction of scanning.

a standard colligative property.^[86] One can suggest that Lys incorporation inhibits the C-T transition in both directions by affecting the rotation of PbBr₆ octahedra.^[87] Lys incorporation hinders this rotation, hence induces a spreading of the phase transformation peak as measured with DSC (Figure 4b) (for more details, see Supporting Information).

The presence of Lys during growth has a noticeable effect on the crystal morphology (Figure 5a,b). As the amount of Lys in the solution increases, the crystals become more cubic-like, with clearer facets and sharper edges and corners. To examine these changes quantitatively, we looked at the diffraction peaks from different reflections of the MAPbBr₃ samples (Figure 5c–e): the

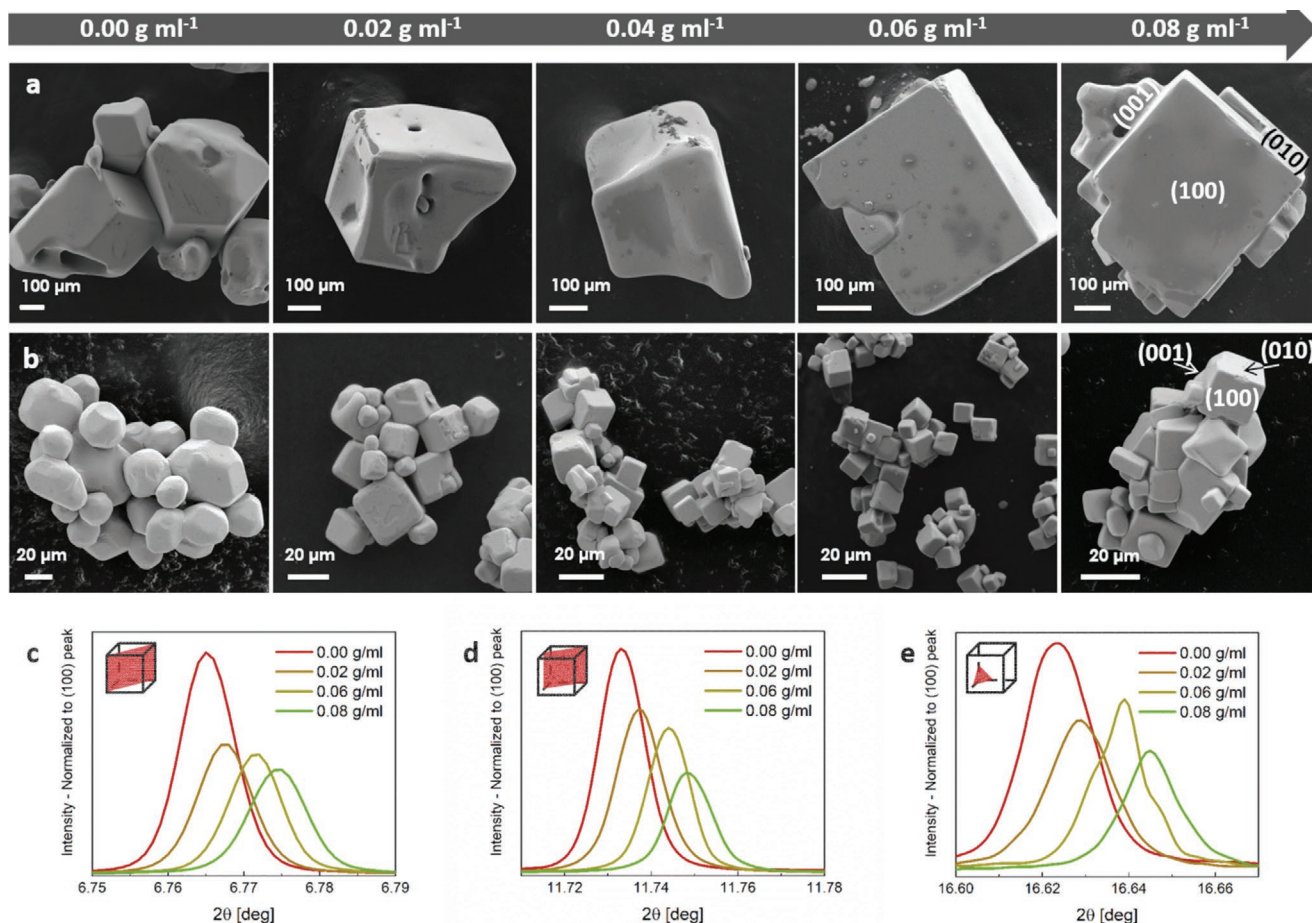


Figure 5. HR-SEM micrographs of MAPbBr₃ crystals grown in the presence of Lys in solution. a) Slow growth; b) Fast growth. The arrow indicates an increase in the concentration of incorporated Lys. c–e) HR-PXRD reflections of different planes of slow-grown MAPbBr₃: c) {110}; d) {120}; e) {222}, grown with different amounts of Lys ($\lambda = 0.49599$ Å). The intensity of the diffraction peaks is normalized to that of the corresponding {100} diffraction peak.

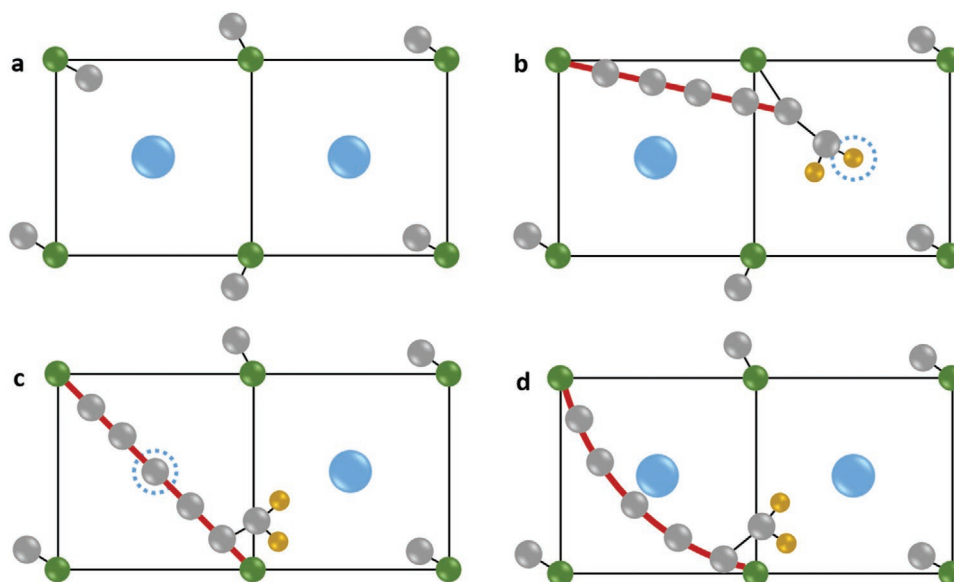


Figure 6. Schematic representation of two neighboring MAPbBr₃ {100} planes. a) Pure MAPbBr₃, b) MAPbBr₃ with Lys incorporated along $\langle 130 \rangle$ during fast growth. c,d) MAPbBr₃ with Lys incorporated along $\langle 110 \rangle$ during slow growth, where Lys backbone c) substitutes Br⁻, and d) bends around Br⁻. The “molecular bridging” of the Lys backbone is marked in red. Color legend: N, green; C, gray; Br, blue; O, gold. The blue dotted line represents a Br⁻ vacancy. H atoms are not presented.

relative intensities of the diffraction peaks from {110}, {120}, and {222} decrease as the Lys incorporation levels increase. Since the intensity of the diffraction peaks is normalized to that of the {100} peak (the most intense diffraction peak in the MAPbBr₃ diffractogram, see Figure S1, Supporting Information), this decrease might also describe the increase in relative intensity of the corresponding {100} diffraction peak. Generally, the presence of Lys leads to an increase in intensity of the {100} reflection. Since the {100} family corresponds to the main facets of the cubic unit cell, this finding corroborates with the observed morphological changes depicted in Figure 5a,b.

The fact that the incorporation of Lys induces higher lattice distortions (in absolute values) than those of any of the other amino acids, combined with the effect of lattice parameter reduction, suggests the following incorporation mechanism: the two NH₃⁺ groups of Lys probably replace two MA⁺ anions in the MAPbBr₃ crystal, similarly to the replacement of carbonate groups in calcite by the COO⁻ group of Asp,^[70] and of Cu²⁺ in Cu₂O.^[75] In the case of MAPbBr₃ the Lys backbone acts as a “molecular bridge” that tightens the atoms together, thereby decreasing the lattice parameter and leading to the reduction in microstrain fluctuations (Figure 2b,c). This bridging effect induces changes in MAPbBr₃ thermal expansion coefficient as well as in its C–T transformation temperature.

A model was developed to understand the possible crystallographic location of Lys incorporated in the MAPbBr₃ crystal, and the level of lattice distortions it induces. The model takes into account the difference between the NH₃⁺–NH₃⁺ distance in Lys, and the MA⁺–MA⁺ distance in the crystal host, along with the ratio of stiffness coefficients of Lys and MAPbBr₃ (for more details, see Supporting Information). We assume two possible modes of incorporation: i) Lys incorporation along the $\langle 130 \rangle$ directions, whereby two NH₃⁺ amino groups of Lys substitute two adjacent MA⁺ ions along the $\langle 100 \rangle$ directions,

while an ionized carboxyl group COO⁻ of Lys substitutes for a Br⁻ anion (Figure 6b). This mode occurs during fast growth at room temperature; ii) Lys molecules are incorporated along the $\langle 110 \rangle$ directions, and can either create a Br⁻ vacancy (Figure 6c) or, more probably, bend around it (Figure 6d). The latter occurs during slow growth at high temperatures. The level of unit cell shrinkage caused by Lys incorporation in these two modes differs: in the case of fast growth (i) $(l_{\text{Lys}} - l_{\langle 130 \rangle})/l_{\langle 130 \rangle} \approx -0.012$, while in the case slow growth (ii) $(l_{\text{Lys}} - l_{\langle 110 \rangle})/l_{\langle 110 \rangle} \approx -0.16$. This indicates that the possible lattice distortions in the case of slow growth can reach up to one order of magnitude higher than those of the fast growth. This allows for substantially high lattice distortions in the case of slow growth even for rather low levels of Lys incorporation (Figure 2b) (for more details see Supporting Information).

Note, that in both cases the incorporation direction is along the unit cell faces, which can explain the passivation of the {100} planes upon Lys incorporation (Figure 5). These suggested mechanisms of Lys incorporation can be also responsible for the difference in incorporation levels between the two growth regimes (Figure 1c): since the incorporation occurs by attachment of Lys molecules to the {100} surface, the incorporation level should be higher for smaller crystals, which exhibit bigger surface area (the case of fast grown crystals). According to Figure 5, this effect is indeed confirmed experimentally. Alternatively, relatively low incorporation levels during slow growth can result from the high lattice distortion required when incorporation is along the $\langle 110 \rangle$ directions.

The remaining question to be answered is: why is incorporation along $\langle 130 \rangle$ is favored during the fast growth, while incorporation along $\langle 110 \rangle$ is favored during the slow growth? One possible explanation is the difference in the solubility of the precursors over temperature. It is known that while Pb(OAc)₂ solubility increases with temperature,^[88] the

solubility of HBr decreases.^[89] In light of this, the Br⁻ supersaturation level in the solution is lower in the fast growth mode as compared to that of the slow growth mode (while the trend is opposite in case of Pb⁺² supersaturation). The low Br⁻ supersaturation level promotes induction of Br⁻ vacancies during MAPbBr₃ precipitation and facilitates substitution of Br⁻ by ionized carboxyl group COO⁻ of Lys in the growing {100} facets of the crystal. This substitution is accompanied by two NH₃⁺ groups of Lys which replace two adjacent MA⁺ ions along <100>, while the Lys backbone inclines along <130>, and therefore mode i) dominates (Figure 6b). At higher temperatures, the HBr solubility in water is lower, and leads to higher Br⁻ supersaturation. Hence, the formation of Br⁻ vacancies in the growing crystal surface is suppressed. In the latter case, the two amino groups of Lys substitute two MA⁺ ions located further apart, i.e., along <110>, while the Lys backbone bends around Br⁻ (Figure 6d). Therefore, mode (ii) dominates.

Next, we investigated the effect of Lys incorporation on the optical properties of the host crystals. To this end, we measured the diffusive reflectance (*R*) spectra of the powdered samples in the visible range (400–700 nm), using a spectrophotometer equipped with an integration sphere. Using the Kubelka-Munk theory, i.e.,^[90,91]

$$F = \frac{(1-R)^2}{2R} \quad (3)$$

where *F* is proportional to the absorption coefficient, and based also on the fact that MAPbBr₃ has a direct bandgap,^[81,82] we plotted (*Fhν*)² versus the photon energy *hν*, taking the bandgap as the x-intercept of the linear part of the plot^[92,93] (see Figure S2 in the Supporting Information).

The incorporation of Lys into MAPbBr₃ indeed induced an increase of more than 1% in its optical bandgap (blueshift) (Figure 7). It is important to note that for a fixed amount of Lys, the change in the bandgap is higher in the case of fast-grown samples, although the lattice distortions (Figure 2b) are lower. For the maximum amount of incorporated Lys in the slow-grown samples (0.3 mol%) the relative change in the

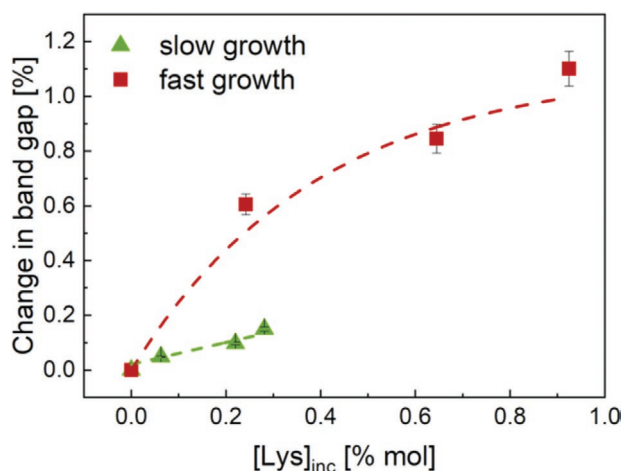


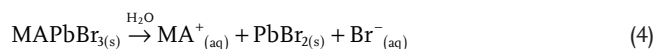
Figure 7. Change in the optical bandgap of MAPbBr₃ versus concentration of incorporated Lys in the case of slow and fast growth.

bandgap is only about 0.1%, that is six times lower than that of the fast-grown samples with similar amount of incorporated Lys. These findings may suggest that the factor governing the change in bandgap is indeed the concentration of incorporated Lys (and the mechanism of incorporation), rather than the induced lattice distortions. This conclusion is consistent with the previously established understanding of the phenomenon^[76] whereby the incorporation of insulating organic molecules induces quantum confinement inside the bulk semiconductor crystals.

The bandgap of the MAPbBr₃ crystals is formed due to an overlap between Pb-6s and Br-5p antibonding atomic orbitals, forming the valence band maximum.^[82] Removing Br⁻, as suggested by incorporation of Lys molecules along <130>, should decrease this overlapping, hence increase the bandgap. The more intensive increase of the bandgap in the fast-grown crystals manifests more substantial removal of Br⁻ anions in the fast crystallization route. Incorporation of Lys molecules along <110> may occur without removal of Br⁻, when Lys molecule is bent. Apparently, such incorporation only slightly affects the electronic structure.

It is interesting to note that changes in the optical bandgap can also originate from changes in hydrostatic volume.^[21,94] In our study, however, this is probably not applicable for two reasons. First, the bandgap deformation potential (i.e., the change in bandgap versus the logarithm of the unit cell volume) is usually positive in HOIPs,^[94,95] as opposed to our results (see Figure S3 in the Supporting Information). Second, a difference between the deformation potentials of the two synthetic routes for the same crystal was clearly seen in our study. Hence, we can conclude that in our case, similarly to that reported in the case of ZnO,^[76] changes observed in the bandgap originate from quantum confinement effects, together with the substitution of Br⁻ anions.

To examine the effect of Lys incorporation on MAPbBr₃ stability, we investigated the dissolution of the hybrid crystals in water. Specifically, we studied the kinetics of crystals dissolution in water using an electrochemical approach, namely by measuring the solution impedance over dissolution time. The dissolution process of MAPbBr₃ crystals results in the release of free ions into the solution:



Hence, the impedance (i.e., resistivity) of the solution decreases due to the increase of the ion concentration. We performed time-dependent impedance measurements for several samples with different incorporation levels of Lys (Figure S5, Supporting Information). The obtained curves were fitted according to Equation (5)

$$\frac{\rho}{\rho_{\min}} = \left[1 - \left(1 - \frac{\rho_{\min}}{\rho_0} \right) \exp\left(-\frac{t}{\tau}\right) \right]^{-1} \quad (5)$$

where τ is the transient time (the time needed to reach a steady-state ion concentration), $\rho_{\min} = 1/\bar{K}\tau$ is the minimum achieved resistivity (the plateau of the plot), \bar{K} is the dissolution rate and ρ_0 is the initial resistivity (prior to the addition of MAPbBr₃).

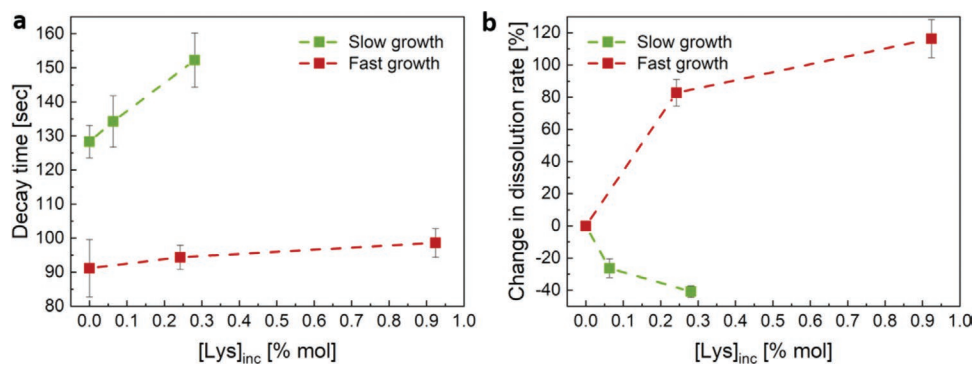


Figure 8. a) Transient time, and b) dissolution rate of MAPbBr₃ in water, measured using time-dependent impedance.

For more details, see Supporting Information. In order to minimize the effect of varying morphology and particle size, all the samples were grinded prior to the measurement.

The change in the transient time of dissolution for the slow- and fast-grown Lys incorporated MAPbBr₃ crystals is presented in **Figure 8a**. In both cases, the transient time increases. As was discussed above, the Lys molecules are located on the {100} planes of the crystal. Hence, it is reasonable to assume that they hinder the ability of the ions to detach and/or attach to the crystal, and increase the time needed to achieve steady state conditions. This effect is much more significant in the case of the slow-grown crystals. The dissolution rate of the fast-grown crystals increases upon addition of Lys (**Figure 8b**). This corroborates our assumption in regards to the pure substitutional mode of Lys incorporation in the fast-grown mode. The weakly bound Lys molecules readily dissolve in water, thereby forming surface defects and enhancing dissolution of Br⁻ anions. On the other hand, the dissolution rate of the slow grown crystals decreases by almost twofold upon the addition of only 0.3 at% of Lys. This may indicate an additional binding of Br⁻ anions to CH₂ groups of Lys molecules incorporated into the MAPbBr₃ lattice (as illustrated in **Figure 6d**).

In order to confirm these results are valid under humid conditions as well (and not only when the crystals are dissolved in water), we measured the XRD of Lys-incorporated MAPbBr₃ samples, after exposure to a controlled humidity environment for different time periods. Each sample was grinded prior to the experiment. The (121) diffraction peak of the PbBr₂ impurity phase (marked in **Figure S6**, Supporting Information)^[96] emerges in the diffractogram of the pure MAPbBr₃ after three days of exposure (**Figure S6a**, Supporting Information). At the same time, in the sample with the low Lys concentration, this diffraction peak appears only after 5 d (**Figure S6b**, Supporting Information), and does not appear at all in the sample with the high Lys concentration (**Figure S6c**, Supporting Information). We used Rietveld refinements to estimate the amount of PbBr₂ phase after one week of exposure to humidity (**Figure 9**). Clearly, the higher the level of Lys incorporation into MAPbBr₃ crystals, the less PbBr₂ forms under humid conditions. Overall, it is apparent that the incorporation of Lys has a noticeable effect on the dissolution kinetics of MAPbBr₃ crystals in water, as well as on their resistance to humidity. Improving the stability of hybrid perovskite crystals can be therefore achieved by incorporating amino acids during slow crystallization at elevated temperatures.

3. Conclusion

This study shows, for the first time, that the possibility of utilizing amino acid incorporation in order to tune the physical properties of crystalline hosts is not restricted to purely inorganic materials. Here we demonstrated a similar phenomenon with a hybrid semiconductor perovskite whose lattice includes both organic and inorganic components.

Incorporation of Lys molecules into the MAPbBr₃ lattice depends on the mode of crystal growth. At high temperatures (slow crystal growth) rather low Lys incorporation levels result in a significant lattice contraction and slight bandgap changes. On the other hand, at lower temperatures (fast crystal growth) the incorporation levels are noticeably higher, and Lys causes opposite effects in the crystals, namely a lower level of lattice contraction and a considerable bandgap increase. This observation can be explained by the two different modes of Lys incorporation into MAPbBr₃ crystals: i) along (130) directions (low temperatures, fast crystal growth); ii) along (110) directions (high temperatures, slow crystal growth). The difference can be explained by the decrease in HBr solubility in water with increasing temperature, which affects the substitution tendency of Br⁻ anions during Lys incorporation. This interpretation is supported by the experimental changes in both the thermal expansion coefficient of MAPbBr₃ crystals and their resistance to dissolution in water upon Lys incorporation.

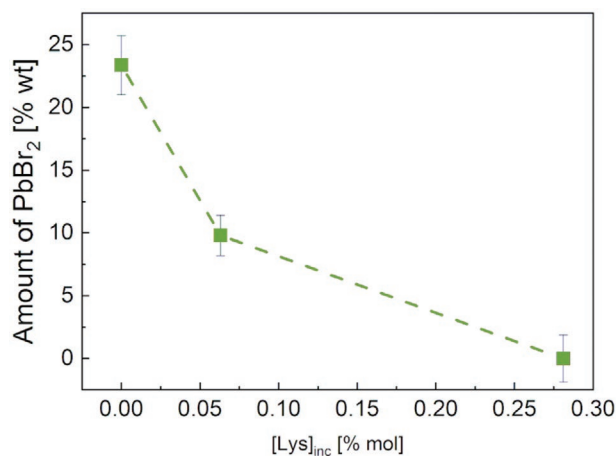


Figure 9. Relative amount of the PbBr₂ impurity phase after a week of exposure to humidity.

Moreover, Lys incorporation has a distinct effect on the stability of MAPbBr₃ in water. While the time required to achieve a steady-state dissolution increases upon the incorporation of Lys in both growth regimes, its incorporation during slow growth decreases MAPbBr₃ dissolution rate by ~40%.

Recently, the addition of amino acids during MAPbBr₃ synthesis was shown to passivate the crystal surface, facilitating the formation of nanocrystals thereby improving devices performance.^[97–99] In our study, we showed that not only do the amino acids passivate the MAPbBr₃ crystal surface, but they also become incorporated into its lattice, thus, alter the optical and thermal properties of the perovskite. Another cardinal outcome of the incorporation is the finding that it can enhance the stability of the host MAPbBr₃ crystal under humid conditions.

We believe that these new discoveries can shed light on the interactions between amino acids and different crystal-line systems. The mechanism of Lys incorporation into a non-oxide hybrid crystal, as shown here, differs from that reported previously, and can provide a new method for fine tuning of bandgap and improved stability of hybrid systems. This latter point will facilitate the commercializing of halide perovskites. Moreover, the observed structural changes induced by such incorporation provide additional evidence for the intriguing interaction between the organic amino acids and the inorganic (or hybrid) crystals, which is still far from being completely understood.

4. Experimental Section

MAPbBr₃ Crystal Growth: Crystals were synthesized according to the method described by Poglitsch and Weber.^[7] In a typical process, a Pb²⁺ solution was prepared by dissolving lead acetate trihydrate (2 g Pb(OAc)₂·3H₂O; Merck) in concentrated hydrobromic acid (10 mL 48% HBr; Sigma Aldrich). Different amounts of all the 20 common L-amino acids were added to the Pb²⁺ solution: L-alanine (Ala), L-arginine (Arg), L-asparagine (Asn), L-aspartic acid (Asp), L-cysteine (Cys), L-glutamic acid (Glu), L-glutamine (Gln), glycine (Gly), L-histidine (His), L-isoleucine (Ile), L-leucine (Leu), L-lysine (Lys), L-methionine (Met), L-phenylalanine (Phe), L-proline (Pro), L-serine (Ser), L-threonine (Thr), L-tryptophan (Trp), L-tyrosine (Tyr), and L-valine (Val). Each solution was stirred until dissolution was complete. Meanwhile, a 1:1 (v/v) stock solution of MA⁺ in HBr was prepared by adding a methylammonium hydroxide (MAOH) solution (40% in H₂O; Merck) dropwise into concentrated HBr, while stirring in an ice/water bath. MAPbBr₃ precipitation was achieved simply by the addition of equimolar volumes of MA⁺ solution into the Pb²⁺ solution. This was done via two routes: fast synthesis, in which the MA⁺ to the Pb²⁺ solution were added at room temperature while stirring, and slow synthesis, in which the MA⁺ to a hot Pb²⁺ solution (in an oil bath at 95 °C) was added and allowed the mixture to cool down naturally. In both cases, after precipitation the orange-hued crystals were filtered, washed with acetone, and dried in air.

Chemical Analysis: Amino acid analysis (AAA) was carried out at AminoLab, Rehovot, Israel. Samples were sonicated in concentrated HBr and then washed several times with HBr and acetone to remove any remaining Lys from the surface. To ensure that no Lys was left after this process, a pure sample (without Lys) was mixed in a Lys-containing HBr solution and subjected it to the same treatment. Samples were filtered and dried in air. Each sample was then dissolved in 0.1% HCl and injected into a column to separate the Lys from the MA⁺ cations that had originated from the crystals. This was followed by postcolumn derivatization with ninhydrin and detection in a standard UV–vis detector.^[100,101]

Structural Characterization: Samples were subjected to high-resolution powder X-ray diffraction (HR-PXRD) in ID22 at the European Synchrotron Radiation Facility (ESRF) in Grenoble, France, at a monochromatic radiation of 0.49599 Å (corresponding to 25 keV). Each sample was transferred to a 0.9 mm glass capillary and scanned three times at a fast rate (10 deg min⁻¹) at three different positions, while being rotated. This setup makes it possible to avoid beam damage and texture influences. The Rietveld refinement method was used in GSAS-II software for data analysis and lattice parameter calculations.^[83] GnuPlot software was used for peak fitting.

Morphology: Crystal morphology was observed by using a Zeiss Ultra Plus high-resolution scanning electron microscope (HR-SEM).

Thermal Properties: The lattice parameter of each sample was measured at different temperatures (290 K, 275 K, 250 K, 230 K) in ID22 at ESRF, as described above. Cooling was achieved with a cold nitrogen gas blower. The lattice expansion coefficient was calculated according to Equation (1), i.e., the slope of ln(*a*) (when *a* is the measured lattice parameter) versus the absolute temperature. To evaluate the phase transformation temperature, DSC was used. Each sample was scanned from room temperature to –80 °C and back, at a rate of 5 °C min⁻¹ (DSC 3+; Mettler Toledo). The transformation temperature was taken as the temperature at onset of the peak.

Optical Properties: The diffusive reflectance (*R*) of the powders was measured in the visible range (400–700 nm) using a spectrophotometer equipped with an integration sphere (Cary 5000, Agilent). According to the Kubelka-Munk theory presented as Equation (3),^[90,91] *F* is proportional to the absorption coefficient.

Hence, based on the fact that MAPbBr₃ has a direct bandgap,^[81,82] (*Fhv*)² was plotted versus the photon energy *hν*, and the bandgap was taken as the x-intercept of the linear part of the plot.^[92,93]

Stability Measurements: The kinetics of MAPbBr₃ crystals solubility was measured in water using a simple electrochemical set-up. A standard reference electrode was immersed in DI water while stirring. The impedance of the solution was measured over time (Gamry Reference 3000), at a constant frequency of 100 kHz and an amplitude of 10 mV. At a known time, a known amount of crushed MAPbBr₃ crystals was added to the solution, and a significant decrease in the resistivity of the solution was observed. The measurement was carried out until reaching a plateau of the impedance versus time curve.

Resistance to Humidity: Grinded samples with different amounts of incorporated Lys were placed in a desiccator, together with a beaker containing a saturated NaCl solution in DI water. Such a solution should provide a relative humidity of ~76%.^[32] The desiccator was sealed and placed in the dark. XRD (Rikagu SmartLab 9 kW, Cu-K α radiation) was collected prior this treatment, and after 3, 5, and 7 d.

Supporting Information

Supporting Information is available from the Wiley Online Library or from the author.

Acknowledgements

The authors acknowledge ID22 beamline at the ESRF (Grenoble, France) and Dr. C. Dejoie and Dr. W. Mashikoane for helping in collecting the powder diffraction data, G. Kozyukin from the Israel Institute of Metals (IIM) for his help with the electrochemical measurements. Additionally, the authors thank Asst. Prof. Yehonadav Bekenstein for the helpful discussions. This research was supported by a Grant from the GIF, the German-Israeli Foundation for Scientific Research and Development No. I-1512-401.10.

Conflict of Interest

The authors declare no conflict of interest.

Keywords

bandgap engineering, bioinspired molecular bridging, hybrid perovskites, perovskite stability

Received: June 17, 2020

Revised: July 20, 2020

Published online:

- [1] Y. Zhao, K. Zhu, *Chem. Soc. Rev.* **2016**, *45*, 655.
- [2] W. Li, Z. Wang, F. Deschler, S. Gao, R. H. Friend, A. K. Cheetham, *Nat. Rev. Mater.* **2017**, *2*, 16099.
- [3] T. M. Brenner, D. A. Egger, L. Kronik, G. Hodes, D. Cahen, *Nat. Rev. Mater.* **2016**, *1*, 15007.
- [4] A. Toshniwal, V. Kheraj, *Sol. Energy* **2017**, *149*, 54.
- [5] M. I. Asghar, J. Zhang, H. Wang, P. D. Lund, *Renewable Sustainable Energy Rev.* **2017**, *77*, 131.
- [6] T. Miyasaka, *Chem. Lett.* **2015**, *44*, 720.
- [7] P. Gao, M. Grätzel, M. K. Nazeeruddin, *Energy Environ. Sci.* **2014**, *7*, 2448.
- [8] X. Tong, F. Lin, J. Wu, Z. M. Wang, *Adv. Sci.* **2016**, *3*, 1500201.
- [9] Y.-H. Kim, H. Cho, J. H. Heo, T.-S. Kim, N. Myoung, C.-L. Lee, S. H. Im, T.-W. Lee, *Adv. Mater.* **2015**, *27*, 1248.
- [10] H. Cho, S.-H. Jeong, M.-H. Park, Y.-H. Kim, C. Wolf, C.-L. Lee, J. H. Heo, A. Sadhanala, N. Myoung, S. Yoo, S. H. Im, R. H. Friend, T.-W. Lee, *Science* **2015**, *350*, 1222.
- [11] Z. Xiao, R. A. Kerner, L. Zhao, N. L. Tran, K. M. Lee, T.-W. Koh, G. D. Scholes, B. P. Rand, *Nat. Photonics* **2017**, *11*, 108.
- [12] L. Dou, Y. (Micheal) Yang, J. You, Z. Hong, W.-H. Chang, G. Li, Y. Yang, *Nat. Commun.* **2014**, *5*, 5404.
- [13] W. Tian, H. Zhou, L. Li, *Small* **2017**, *13*, 1702107.
- [14] N. J. Jeon, J. H. Noh, Y. C. Kim, W. S. Yang, S. Ryu, S. Il Seok, *Nat. Mater.* **2014**, *13*, 897.
- [15] M. A. Green, K. Emery, Y. Hishikawa, W. Warta, E. D. Dunlop, *Prog. Photovoltaics Res. Appl.* **2015**, *23*, 1.
- [16] P. K. Nayak, S. Mahesh, H. J. Snaith, D. Cahen, *Nat. Rev. Mater.* **2019**, *4*, 269.
- [17] A. Poglitsch, D. Weber, *J. Chem. Phys.* **1987**, *87*, 6373.
- [18] M. I. Saidaminov, A. L. Abdelhady, B. Murali, E. Alarousu, V. M. Burlakov, W. Peng, I. Dursun, L. Wang, Y. He, G. Maculan, A. Goriely, T. Wu, O. F. Mohammed, O. M. Bakr, *Nat. Commun.* **2015**, *6*, 7586.
- [19] R. K. Singh, R. Kumar, A. Kumar, N. Jain, R. K. Singh, J. Singh, *J. Alloys Compd.* **2018**, *743*, 728.
- [20] B. R. Sutherland, E. H. Sargent, *Nat. Photonics* **2016**, *10*, 295.
- [21] A. Walsh, *J. Phys. Chem. C* **2015**, *119*, 5755.
- [22] C.-X. Zhang, T. Shen, D. Guo, L.-M. Tang, K. Yang, H.-X. Deng, *InfoMat* **2020**, *1*.
- [23] R. Wang, M. Mujahid, Y. Duan, Z. Wang, J. Xue, Y. Yang, *Adv. Funct. Mater.* **2019**, *29*, 1808843.
- [24] H.-S. Kim, J.-Y. Seo, N.-G. Park, *ChemSusChem* **2016**, *9*, 2528.
- [25] B. Brunetti, C. Cavallo, A. Ciccio, G. Gigli, A. Latini, *Sci. Rep.* **2016**, *6*, 31896.
- [26] A. M. A. Leguy, Y. Hu, M. Campoy-Quiles, M. I. Alonso, O. J. Weber, P. Azarhoosh, M. van Schilfgaarde, M. T. Weller, T. Bein, J. Nelson, P. Docampo, P. R. F. Barnes, *Chem. Mater.* **2015**, *27*, 3397.
- [27] J. Yang, B. D. Siempelkamp, D. Liu, T. L. Kelly, *ACS Nano* **2015**, *9*, 1955.
- [28] N. Aristidou, I. Sanchez-Molina, T. Chotchuangchutchaval, M. Brown, L. Martinez, T. Rath, S. A. Haque, *Angew. Chem., Int. Ed.* **2015**, *54*, 8208.
- [29] E. J. Juarez-Perez, L. K. Ono, M. Maeda, Y. Jiang, Z. Hawash, Y. Qi, *J. Mater. Chem. A* **2018**, *6*, 9604.
- [30] L. Zheng, Y.-H. Chung, Y. Ma, L. Zhang, L. Xiao, Z. Chen, S. Wang, B. Qu, Q. Gong, *Chem. Commun.* **2014**, *50*, 11196.
- [31] J. Wang, Y. Chen, M. Liang, G. Ge, R. Zhou, Z. Sun, S. Xue, *Dye. Pigment.* **2016**, *125*, 399.
- [32] G. Abdelmageed, H. R. Sully, S. Bonabi Naghadah, A. El-Hag Ali, S. A. Carter, J. Z. Zhang, *ACS Appl. Energy Mater.* **2018**, *1*, 387.
- [33] J. You, L. Meng, T.-B. Song, T.-F. Guo, Y. (Michael) Yang, W.-H. Chang, Z. Hong, H. Chen, H. Zhou, Q. Chen, Y. Liu, N. De Marco, Y. Yang, *Nat. Nanotechnol.* **2016**, *11*, 75.
- [34] S. Zou, Y. Liu, J. Li, C. Liu, R. Feng, F. Jiang, Y. Li, J. Song, H. Zeng, M. Hong, X. Chen, *J. Am. Chem. Soc.* **2017**, *139*, 11443.
- [35] B. Kim, S. Il Seok, *Energy Environ. Sci.* **2020**, *13*, 805.
- [36] Y. Li, L. Meng, Y. Yang, G. Xu, Z. Hong, Q. Chen, J. You, G. Li, Y. Yang, Y. Li, *Nat. Commun.* **2016**, *7*, 10214.
- [37] X. Li, M. Ibrahim Dar, C. Yi, J. Luo, M. Tschumi, S. M. Zakeeruddin, M. K. Nazeeruddin, H. Han, M. Grätzel, *Nat. Chem.* **2015**, *7*, 703.
- [38] A. Kirakosyan, S. Yun, S.-G. Yoon, J. Choi, *Nanoscale* **2018**, *10*, 1885.
- [39] J. Yin, J. Cao, X. He, S. Yuan, S. Sun, J. Li, N. Zheng, L. Lin, *J. Mater. Chem. A* **2015**, *3*, 16860.
- [40] C. Sanchez, H. Arribart, M. M. Giraud Guille, *Nat. Mater.* **2005**, *4*, 277.
- [41] G. Mayer, *Science* **2005**, *310*, 1144.
- [42] L. A. Estroff, A. D. Hamilton, *Chem. Mater.* **2001**, *13*, 3227.
- [43] F. Nudelman, N. A. J. M. Sommerdijk, *Angew. Chem., Int. Ed.* **2012**, *51*, 6582.
- [44] D. L. Feldheim, B. E. Eaton, *ACS Nano* **2007**, *1*, 154.
- [45] P. Fratzl, O. Kolednik, F. D. Fischer, M. N. Dean, *Chem. Soc. Rev.* **2016**, *45*, 252.
- [46] A. R. Studart, *Adv. Mater.* **2012**, *24*, 5024.
- [47] A. Hirsch, D. Gur, I. Polishchuk, D. Levy, B. Pokroy, A. J. Cruz-Cabeza, L. Addadi, L. Kronik, L. Leiserowitz, *Chem. Mater.* **2015**, *27*, 8289.
- [48] I. C. Olson, A. Z. Blonsky, N. Tamura, M. Kunz, B. Pokroy, C. P. Romao, M. A. White, P. U. P. A. Gilbert, *J. Struct. Biol.* **2013**, *184*, 454.
- [49] E. Seknazi, B. Pokroy, *Adv. Mater.* **2018**, *30*, 1707263.
- [50] E. Zolotoyabko, *Adv. Mater. Interfaces* **2017**, *4*, 1600189.
- [51] I. Polishchuk, A. A. Bracha, L. Bloch, D. Levy, S. Kozachkevich, Y. Etinger-Geller, Y. Kauffmann, M. Burghammer, C. Giacobbe, J. Villanova, G. Hendler, C.-Y. Sun, A. J. Giuffrè, M. A. Marcus, L. Kundanati, P. Zaslansky, N. M. Pugno, P. U. P. A. Gilbert, A. Katsman, B. Pokroy, *Science (80-)* **2017**, *358*, 1294.
- [52] H. Li, H. L. Xin, M. E. Kunitake, E. C. Keene, D. A. Muller, L. A. Estroff, *Adv. Funct. Mater.* **2011**, *21*, 2028.
- [53] M. E. Kunitake, L. M. Mangano, J. M. Peloquin, S. P. Baker, L. A. Estroff, *Acta Biomater.* **2013**, *9*, 5353.
- [54] E. Seknazi, S. Kozachkevich, I. Polishchuk, N. Bianco Stein, J. Villanova, J.-P. Suuronen, C. Dejoie, P. Zaslansky, A. Katsman, B. Pokroy, *Nat. Commun.* **2019**, *10*, 4559.
- [55] A. Herman, L. Addadi, S. Weiner, *Nature* **1988**, *331*, 546.
- [56] A. Berman, L. Addadi, A. Kivick, L. Leiserowitz, M. Nelson, S. Weiner, *Science* **1990**, *250*, 664.
- [57] B. Jones, *Sediment. Geol.* **2017**, *353*, 64.
- [58] E. Weber, L. Bloch, C. Guth, A. N. Fitch, I. M. Weiss, B. Pokroy, *Chem. Mater.* **2014**, *26*, 4925.
- [59] A. Hanisch, P. Yang, A. N. Kulak, L. A. Fielding, F. C. Meldrum, S. P. Armes, *Macromolecules* **2016**, *49*, 192.
- [60] C. T. Hendley, L. A. Fielding, E. R. Jones, A. J. Ryan, S. P. Armes, L. A. Estroff, *J. Am. Chem. Soc.* **2018**, *140*, 7936.
- [61] B. Kahr, R. W. Gurney, *Chem. Rev.* **2001**, *101*, 893.
- [62] G. Magnabosco, I. Polishchuk, F. Palomba, E. Rampazzo, L. Prodi, J. Aizenberg, B. Pokroy, G. Falini, *Cryst. Growth Des.* **2019**, *19*, 4429.
- [63] A. N. Kulak, M. Semsarilar, Y.-Y. Kim, J. Ihli, L. A. Fielding, O. Cespedes, S. P. Armes, F. C. Meldrum, *Chem. Sci.* **2014**, *5*, 738.

- [64] Y. Liu, W. Yuan, Y. Shi, X. Chen, Y. Wang, H. Chen, H. Li, *Angew. Chem., Int. Ed.* **2014**, *53*, 4127.
- [65] M. Di Giosia, I. Polishchuk, E. Weber, S. Fermani, L. Pasquini, N. M. Pugno, F. Zerbetto, M. Montalti, M. Calvaresi, G. Falini, B. Pokroy, *Adv. Funct. Mater.* **2016**, *26*, 5569.
- [66] G. Magnabosco, M. Di Giosia, I. Polishchuk, E. Weber, S. Fermani, A. Bottoni, F. Zerbetto, P. G. Pelicci, B. Pokroy, S. Rapino, G. Falini, M. Calvaresi, *Adv. Healthcare Mater.* **2015**, *4*, 1510.
- [67] X. Jin, L. Chen, Y. Liu, T. Ye, C. Hu, J. Ren, H. Chen, H. Li, *J. Phys. Chem. C* **2019**, *123*, acs.jpcc.9b02329.
- [68] H. Li, H. L. Xin, D. A. Muller, L. A. Estroff, *Science* **2009**, *326*, 1244.
- [69] S. Borukhin, L. Bloch, T. Radlauer, A. H. Hill, A. N. Fitch, B. Pokroy, *Adv. Funct. Mater.* **2012**, *22*, 4216.
- [70] Y.-Y. Kim, J. D. Carloni, B. Demarchi, D. Sparks, D. G. Reid, M. E. Kunitake, C. C. Tang, M. J. Duer, C. L. Freeman, B. Pokroy, K. Penkman, J. H. Harding, L. A. Estroff, S. P. Baker, F. C. Meldrum, *Nat. Mater.* **2016**, *15*, 903.
- [71] S. Mijowska, I. Polishchuk, A. Lang, E. Seknazi, C. Dejoie, S. Fermani, G. Falini, N. Demitri, M. Polentarutti, A. Katsman, B. Pokroy, *Chem. Mater.* **2020**, *32*, 4205.
- [72] C. L. Chen, J. Qi, J. Tao, R. N. Zuckermann, J. J. Deyoreo, *Sci. Rep.* **2015**, *4*, 6266.
- [73] Y. Y. Kim, J. D. Carloni, B. Demarchi, D. Sparks, D. G. Reid, M. E. Kunitake, C. C. Tang, M. J. Duer, C. L. Freeman, B. Pokroy, K. Penkman, J. H. Harding, L. A. Estroff, S. P. Baker, F. C. Meldrum, *Nat. Mater.* **2016**, *15*, 903.
- [74] A. Brif, G. Ankonina, C. Drathen, B. Pokroy, *Adv. Mater.* **2014**, *26*, 477.
- [75] I. Polishchuk, N. Bianco-Stein, A. Lang, M. Kurashvili, M. Caspary Toroker, A. Katsman, J. Feldmann, B. Pokroy, *Adv. Funct. Mater.* **2020**, *30*, 1910405.
- [76] M. A. H. Muhammed, M. Lamers, V. Baumann, P. Dey, A. J. Blanch, I. Polishchuk, X.-T. Kong, D. Levy, A. S. Urban, A. O. Govorov, B. Pokroy, J. Rodríguez-Fernández, J. Feldmann, *J. Phys. Chem. C* **2018**, *122*, 6348.
- [77] N. J. Jeon, J. H. Noh, W. S. Yang, Y. C. Kim, S. Ryu, J. Seo, S. Il Seok, *Nature* **2015**, *517*, 476.
- [78] M. Kulbak, S. Gupta, N. Kedem, I. Levine, T. Bendikov, G. Hodes, D. Cahen, *J. Phys. Chem. Lett.* **2016**, *7*, 167.
- [79] H. Wei, Y. Fang, P. Mulligan, W. Chirrazzi, H.-H. Fang, C. Wang, B. R. Ecker, Y. Gao, M. A. Loi, L. Cao, J. Huang, *Nat. Photonics* **2016**, *10*, 333.
- [80] A. D. Wright, C. Verdi, R. L. Milot, G. E. Eperon, M. A. Pérez-Osorio, H. J. Snaith, F. Giustino, M. B. Johnston, L. M. Herz, *Nat. Commun.* **2016**, *7*, 11755.
- [81] K.-H. Wang, L.-C. Li, M. Shellaiah, K. Wen Sun, *Sci. Rep.* **2017**, *7*, 13643.
- [82] X. Chen, R. Meng, J. Jiang, Q. Liang, Q. Yang, C. Tan, X. Sun, S. Zhang, T. Ren, *Phys. Chem. Chem. Phys.* **2016**, *18*, 16302.
- [83] B. H. Toby, R. B. Von Dreele, *J. Appl. Crystallogr.* **2013**, *46*, 544.
- [84] E. Zolotoyabko, *Basic Concepts of X-ray Diffraction*, Wiley-VCH, Weinheim **2014**.
- [85] B. Pokroy, A. N. Fitch, E. Zolotoyabko, *Adv. Mater.* **2006**, *18*, 2363.
- [86] D. V. Ragone, *Thermodynamics of Materials*, John Wiley & Sons, Ltd., New York **2000**.
- [87] Y. Kawamura, H. Mashiyama, K. Hasebe, *J. Phys. Soc. Jpn.* **2002**, *71*, 1694.
- [88] A. Seidell, W. F. Linke, *J. Am. Med. Assoc.* **1928**, *91*, 1131.
- [89] D. R. Gaskell, D. E. Laughlin, *Introduction to the Thermodynamics of Materials*, 6th ed., Taylor & Francis, London **2018**.
- [90] P. Kubelka, F. Munk, *Z. Tech. Phys.* **1931**, *12*, 593.
- [91] R. López, R. Gómez, *J. Sol-Gel Sci. Technol.* **2012**, *61*, 1.
- [92] J. Tauc, R. Grigorovici, A. Vancu, *Phys. Status Solidi B* **1966**, *15*, 627.
- [93] J. Tauc, *Mater. Res. Bull.* **1968**, *3*, 37.
- [94] J. M. Frost, K. T. Butler, F. Brivio, C. H. Hendon, M. van Schilfgaarde, A. Walsh, *Nano Lett.* **2014**, *14*, 2584.
- [95] I. Borriello, G. Cantele, D. Ninno, *Phys. Rev. B* **2008**, *77*, 235214.
- [96] R. W. G. Wyckoff, *Crystal Structures*, Robert E. Krieger Publication Company, Malabar, FL **1982**.
- [97] B. Luo, S. B. Naghadeh, A. Allen, X. Li, J. Z. Zhang, *Adv. Funct. Mater.* **2017**, *27*, 1604018.
- [98] D. Jia, J. Chen, M. Yu, J. Liu, E. M. J. Johansson, A. Hagfeldt, X. Zhang, *Small* **2020**, *16*, 2001772.
- [99] Y. C. Shih, Y. B. Lan, C. S. Li, H. C. Hsieh, L. Wang, C. I. Wu, K. F. Lin, *Small* **2017**, *13*, 1604305.
- [100] W. H. Fitzpatrick, *Science* **1949**, *109*, 469.
- [101] M. Stanford, H. S. William, *J. Biol. Chem.* **1948**, *367*.